

## **Timescale Analysis of Marine Boundary Layer Aerosol Evolution:**

### **Lagrangian Case Studies Under Clean and Polluted Cloudy Conditions.**

**Claudia Hoell and Colin O'Dowd**

*Centre for Marine and Atmospheric Sciences,  
School of Sciences, University of Sunderland,  
Sunderland SR2 7BW, U.K*

**Simon Osborne and Doug Johnson**

*Meteorological Research Flight,  
DERA, Farnborough, Hampshire  
GUI, UK*

#### **Abstract**

Significant changes were observed in the sub-micron aerosol size distribution during a clean and a polluted Lagrangian study of marine boundary layer (MBL) aerosol and meteorological evolution during ACE-2. These changes were accompanied by significant alterations in boundary layer meteorology and structure. The clean case (LAG1) shows a reduction in the fine mode aerosol from  $1050 \text{ cm}^{-3}$  to  $750 \text{ cm}^{-3}$  and an increase in the accumulation mode concentration from  $76 \text{ cm}^{-3}$  to  $162 \text{ cm}^{-3}$  over 26 hours. Dominant meteorological features during the same period comprised a reduction in boundary layer height from  $\approx 1500 \text{ m}$  to  $\approx 800 \text{ m}$  and an increase in the surface layer wind speed from  $5 \text{ m s}^{-1}$  to  $15 \text{ m s}^{-1}$ . A detailed time scale analysis, based upon measured data and including processes such as coagulation, condensation, deposition, chemical processing, sea-salt flux and entrainment, suggests that the dominant loss process for fine mode aerosol is coagulation, while the enhancement of accumulation mode aerosol can be almost totally ascribed to enhanced sea-salt aerosol flux into the reduced mixed layer volume. Aerosol size distributions from the polluted Lagrangian (LAG2) indicated little growth in particle diameter, and both fine and accumulation mode were observed to decrease in concentration from  $2700 \text{ cm}^{-3}$  to  $1150 \text{ cm}^{-3}$  and from  $670 \text{ cm}^{-3}$  to  $430 \text{ cm}^{-3}$  in 26 hours, respectively. Dilution with cleaner free tropospheric air as the boundary layer height increased from  $\approx 500 \text{ m}$  to  $> 1000 \text{ m}$  is suggested to be the primary factor relating to reduced aerosol concentrations in this case. To a smaller extent, coagulation and precipitation scavenging were calculated to be of some importance. For both Lagrangian case studies, meteorological changes, followed by physical aerosol-cloud interactions, appear to have the greatest influence on the MBL aerosol size distribution and number concentration over the given timescale.

*In press, Tellus, ACE-2 Special Issue 1999*

*Corresponding Author – Colin O'Dowd  
Email: [colin.odowd@emas.demon.co.uk](mailto:colin.odowd@emas.demon.co.uk)*

## 1. Introduction

Atmospheric aerosols contribute to the radiative budget of the earth directly by scattering and absorbing incoming solar radiation and indirectly by influencing the microphysical, and consequently, the optical properties and the lifetime of clouds (e. g. IPCC 1995). Alterations in number concentration, size distribution or chemical composition of the aerosol may therefore have considerable impact on the net flux of radiation through the earth's atmosphere. An important example is the interaction between aerosols and maritime stratiform clouds, which cover large areas of the ocean and whose albedo is much higher than that of the sea surface (Slingo, 1990). Because of the low susceptibility of these clouds, aerosols can have a strong effect on their properties (O'Dowd et al., 1999a; O'Dowd et al., 1999b, Durkee et al. 1999). While the aerosol influences clouds, they in turn can have an impact on aerosol physical and chemical properties. For example, Hoppel et al. (1986) and Hoppel et al. (1994) illustrated how the passage of aerosol through clouds leads to the development of a bi-modal size distribution with a fine mode (mode diameter  $d \approx 30\text{-}60$  nm) and an accumulation mode ( $d \approx 150\text{-}250$  nm). This process was attributed to particle growth by aqueous phase oxidation of dissolved trace gases in activated cloud droplets, especially the oxidation of  $\text{SO}_2$  by hydrogen peroxide and ozone in cloud liquid water. O'Dowd et al. (1999c) found that, under favourable conditions, the accumulation mode aerosol gradually grew in mean diameter after successive passages through marine stratocumulus. Comparison with modelling studies showed, that the measurements could be explained by liquid-phase sulphate production in cloud.

Aerosols are also subject to several microphysical and chemical processes in the cloud-free atmosphere, influencing both particle number concentration and size distribution. Particles are removed from or added to the spectrum by dry deposition (Sievering et al., 1992), precipitation scavenging (Hoppel et al., 1994), mixing between air masses of boundary layer and tropospheric origin (Raes, 1995) or the production of sea-salt particles (O'Dowd et al., 1996). Loss and gain rates sensitive to particle size. Mechanisms such as diffusive coagulation, self-coagulation, condensation growth and chemical processing, add mass to particles that are already part of the spectrum, thus causing a shift towards larger dry diameters.

To study the relative importance of these processes in shaping the aerosol size distribution in the marine boundary layer (MBL), airborne Lagrangian experiments were conducted during the ACE-2 field campaign (Raes et al., this issue) in both clean and polluted air. Johnson et al. a (this issue) give a full description of the experimental design and rationale of the Lagrangian studies. In summary, an air mass was tagged using an inert tracer and smart balloons released from the research ship R / V Vodyanitsky, and for the following 26 hours, airborne measurements were conducted in the same air parcel. This allowed observations of the evolution of boundary layer thermodynamics, aerosol and cloud microphysical and chemical properties over nearly 30 hours.

Before performing detailed process-model studies of the aerosol evolution during the Lagrangians, it is useful to estimate the relative importance of different mechanisms under the specific conditions present during the experiments. Calculating particle loss, production and growth rates in a time scale analysis, based on measured MBL and aerosol features, allows the most dominant processes to be identified at an early stage. This paper presents such an analysis for the ACE-2 clean and polluted Lagrangian experiments (LAG1, LAG2). No analysis is presented for the second polluted Lagrangian experiment (LAG3), since negligible aerosol evolution was observed (Wood et al, this issue).

## 2. Processes and Time Scale Calculations

### 2.1 Dry Deposition

Dry deposition summarises all mechanisms, by which particles and gas species are removed from the atmosphere in absence of precipitation. It is mainly dominated by surface properties, turbulent features and shape, size and density of the particles. A simple approach to estimate the removal rate  $(dN / dt)_D$  of particles by dry deposition flux per unit time is (Smith et al., 1990)

$$\left( \frac{dN}{dt} \right)_D = -v_d N h_m^{-1} \quad (1).$$

All parameters influencing the removal process are included in the dry deposition velocity  $v_d$ . Values for  $v_d$  as a function of particle diameter and wind speed were derived from experimental data by Slinn et al. (1978).  $N$  is the average number concentration of particles in the mixing volume with altitude  $h_m$ . For this analysis,  $h_m$  is assumed to be the height of the well-mixed surface layer.

## 2.2 Precipitation Scavenging

Precipitation scavenging describes the removal of particles from the atmosphere by collision with rain drops. The number removal rate of aerosol due to scavenging below precipitating clouds is (Seinfeld and Pandis, 1997)

$$\frac{dN}{dt} = -L_n N \quad (2)$$

For the simplified scenario of a monodisperse aerosol being scavenged by a monodisperse droplet mode, the mean number scavenging coefficient  $L_n$  is proportional to the collision efficiency between particles and rain drops and the drop falling velocity.

## 2.3 Sea-salt production

An upwards flux of sea-salt aerosol, formed by the bursting of small bubbles at the sea surface (Blanchard, 1980), is considered to enhance the concentration of sub-micrometer aerosol in the clean MBL (e.g., O'Dowd and Smith, 1993, Murphy et al., 1998). Nilsson et al. (1998) suggest a relation

$$\log \langle N' w' \rangle = ku - m$$

between wind speed  $u$  in  $\text{m s}^{-1}$  and the flux  $\langle N' w' \rangle$  in  $10^6 \text{ m}^{-2} \text{ s}^{-1}$  of salt particles from the sea surface, where  $N'$  and  $w'$  are small-scale fluctuations in the number of particles per  $\text{m}^3$  and the vertical wind speed component, respectively. The regression parameters  $k$  and  $m$  were derived from fits of the flux-relation to data measured by Nilsson et al. (1998). The production rate for sea-salt particles in  $\text{cm}^{-3} \text{ s}^{-1}$  is

$$\frac{dN}{dt} = 10^{ku-m} (h_{MBL})^{-1} \quad (3)$$

where  $k = 0.217$  and  $m = 2.79$ . Production rates and resulting increases in number concentration are calculated taking into account the evolution of the MBL height  $h_{MBL}$  and the surface layer wind speed over the observed periods.

## 2.4 Mixing of MBL and free tropospheric air

An increase in the MBL volume due to a rising subsidence inversion causes mixing of MBL and free tropospheric air. As particle concentrations in both air masses are usually different, the concentration in the MBL will reach a new value  $N_M$ . In a simplified approach,  $N_M$  can be determined from the mean of the initial concentrations in the MBL  $N$  and in the free troposphere  $N_{FT}$ , weighted by the original height of the MBL  $h_{MBL}$  and the increase in height  $\Delta h$

$$N_M = (Nh_S + N_{FT} \Delta h) (h_S + \Delta h)^{-1} \quad (4)$$

with  $\Delta h = h_E - h_S$ ,  $h_S$  and  $h_E$  are heights of the subsidence inversion at begin and end of the observed period of time. This estimation assumes mixing over the whole MBL and only takes into account large-scale average changes in particle concentrations. It neglects the complex processes involved in the local entrainment process at the subsidence inversion (e. g., Nicholls and Leighton, 1986).

## 2.5 Coagulation

To calculate coagulation loss rates for particles, a simplified model of two monodisperse fractions of particles with concentrations  $N_1$ ,  $N_2$  and diameters  $d_1$ ,  $d_2$  ( $d_1 < d_2$ ) can be applied. In this case, the coagulation rate, quantifying the reduction in  $N_1$  due to coagulation with particles ( $N_2$ ,  $d_2$ ) per unit time, is (Seinfeld and Pandis, 1997)

$$\frac{dN_1}{dt} = -N_1 N_2 K_{12} \quad (5)$$

with coagulation coefficients  $K_{12}$  as a function of  $d_1$ ,  $d_2$ . Coagulation causes an increase in mass  $m_2$  and therefore acts as a growth mechanism for particle category 2. With the mass balance

$$-\frac{dm_1}{dt} = \frac{dm_2}{dt} \approx \frac{m_2(t + \Delta t) - m_2(t)}{\Delta t}$$

and

$$\frac{dm_1}{dt} = \frac{1}{6} \rho d_1^3 \mathbf{r}_p \frac{dN_1}{dt}$$

$\mathbf{r}_p$  referring to the particle density, the growth time  $t_D = \Delta t$  for a single particle 2 from  $d_{21}$  to  $d_{22}$  is

$$t_D = (K_{12}N_1)^{-1} \frac{d_{22}^3 - d_{21}^3}{d_1^3} \quad (6),$$

assuming that  $N_1$  does not change significantly during the growth process. For the following analysis, three types of coagulation are considered. Diffusive coagulation between particle populations **1** and **2** acts as a loss mechanism for mode **1**. Simultaneously, particles of mode **2** increase in size by taking up the mass removed from mode **1**. For example, particles with diameters just below the accumulation mode (i.e. the largest sized fine mode particles) are thus capable of growing into the accumulation mode by diffusive coagulation of smaller fine mode particles. As coagulation coefficients are strongly size dependent, the effectiveness of the process is significantly enhanced in cloud, where some of the particles below the accumulation mode can also be activated into cloud droplets with sizes in the  $\mu\text{m}$ -range. However, in the analysis reported later, we chose to examine growth of particles just above the fine-accumulation mode partition into the mid-to-higher size regimes of the accumulation mode since this growth timescale is more rapid than for those lying below the partition.

Self-coagulation, i. e., coagulation of particles or cloud droplets within one mode ( $d_1 = d_2$ ), is described by a slightly modified version of Equation 2 (Seinfeld and Pandis, 1997)

$$\frac{dN_1}{dt} = -0.5N_1^2K_{11} \quad (7)$$

with the self-coagulation coefficient  $K_{11}$ . This study includes the following coagulation processes:

- Cloud-free diffusive coagulation of the fine mode with larger aerosol modes;
- In-cloud diffusive coagulation between the fine mode and cloud droplets;
- Self-coagulation within each mode (i.e. fine, accumulation and cloud droplet mode).

Coagulation with coarse mode particles ( $d > 500 \text{ nm}$ ), apart from cloud droplets, is neglected. Coalescence resulting from scavenging by large falling droplets is ignored in cloud, but is accounted for in precipitation scavenging below cloud.

## 2.6 Condensation Growth

Oxidation of  $\text{SO}_2$  by OH radicals leads to the formation of Sulphuric acid  $\text{H}_2\text{SO}_4$ , which readily condenses on particles. Previously measured peak OH concentrations for cloud free conditions at near-similar latitudes are typically of the order of  $5 \times 10^6 \text{ molecules cm}^{-3}$  while for cloudy conditions, there are of the order of  $10^6 \text{ cm}^{-3}$  or less (H. Berresheim, personal communications). As no measurements of OH were available for this particular experiment, a typical value for the MBL of  $10^6 \text{ molecules cm}^{-3}$  (Lin et al., 1992, Seinfeld and Pandis, 1997) is used. However, an average concentration of  $10^6 \text{ cm}^{-3}$  over the duration of the experiment is very unlikely and growth timescales derived for OH-related processes must be considered as an upper limit for the relevant rate. The net production rate for  $\text{H}_2\text{SO}_4$  in the gas-phase is

$$\frac{d[\text{H}_2\text{SO}_4]}{dt} = k[\text{SO}_2][\text{OH}] - 2pd_s D[\text{H}_2\text{SO}_4]N_s \left(1 + \frac{8l}{3ad_s}\right)^{-1} \quad (8).$$

The first term on the right hand side describes the  $\text{H}_2\text{SO}_4$ -formation, the reaction rate  $k$  for the oxidation reaction being  $k = 1.2 \times 10^{-12} \text{ cm}^3 \text{ per molecule and second}$  (Atkinson et al., 1989). The second term quantifies the loss rate of  $\text{H}_2\text{SO}_4$  to a constant surface area sink of particles with diameter  $d_s$  and concentration  $N_s$  and is taken from Schwartz (1986). Parameters are diffusion coefficient  $D$  and mean free path  $l$  of  $\text{H}_2\text{SO}_4$  in air and the sticking coefficient  $a$ . Under steady state conditions, i. e.,  $d[\text{H}_2\text{SO}_4]/dt = 0$ , the concentration  $[\text{H}_2\text{SO}_4]$  can be calculated after Equation 8. The condensation growth rate  $dd/dt$  of a fine mode particle can be determined by setting the loss term of Equation 8 equal to the change in particle mass, expressed as the change in dry particle diameter  $d_{dry}$

$$0.5r_{\text{H}_2\text{SO}_4} d_{dry}^2 \frac{dd}{dt} = d_{wet} D m_{\text{H}_2\text{SO}_4} [\text{H}_2\text{SO}_4] \left(1 + \frac{8l}{3ad_{wet}}\right)^{-1} \quad (9).$$

$m_{\text{H}_2\text{SO}_4}$  is the mass of one molecule of  $\text{H}_2\text{SO}_4$  and  $r_{\text{H}_2\text{SO}_4}$  the  $\text{H}_2\text{SO}_4$  - density.

## 2.7 Aqueous-phase chemistry

In an aqueous solution with  $\text{pH} > 3$ , all  $\text{SO}_2$  is dissolved into S(IV) species. S(IV) can be converted to S(VI) by aqueous-phase oxidation reactions, triggered mainly by  $\text{H}_2\text{O}_2$  and  $\text{O}_3$ . When these reactions occur in deliquescent aerosols or cloud droplets, they effectively grow the particle solute mass by increasing the amount of  $\text{SO}_4^{2-}$  in the liquid / solid phase. This  $\text{SO}_4^{2-}$  contributes to the particle mass in the form of Sulphuric acid or salts (Lin et al., 1992). The growth rate, derived from the mass balance between change in dry particle mass and production rate  $A$  in Mol per unit volume and time of  $\text{SO}_4^{2-}$  is

$$\frac{dd}{dt} = \frac{1}{3} \frac{M_p}{r_p} \frac{d_{amb}^3}{d_{dry}^2} A \quad (10)$$

where  $d_{amb}$  denotes either the ambient particle diameter when the air parcel is out of cloud or the cloud droplet diameter when in cloud.  $M_p$  and  $r_p$  are molar mass and density of the substance that forms the particle. Depending on the amount of ammonia available, this will be Sulphuric acid  $\text{H}_2\text{SO}_4$ , ammonium bisulphate  $\text{NH}_4\text{HSO}_4$  or ammonium sulphate  $(\text{NH}_4)_2\text{SO}_4$  (Seinfeld and Pandis, 1997). For the time-scale calculations, formation of ammonium bisulphate with  $M_p = 115 \times 10^{-3} \text{ kg mol}^{-1}$  and  $r_p = 1.78 \times 10^3 \text{ kg m}^{-3}$  is assumed.  $A$  is given by Lin et al. (1992) as

$$A = k_6 [\text{H}_2\text{O}_2][\text{SO}_2] + k_7 [\text{O}_3][\text{SO}_2](1 + K_4[\text{H}^+]^{-1} + K_4 K_5[\text{H}^+]^{-2})$$

with reaction rates  $k_i$  and equilibrium constants  $K_i$  for the main conversion reactions from S(IV) to S(VI). Solving Equation 10 delivers a relationship for the growth time from dry diameter  $d_0$  to  $d_1$

$$t_{IC} = r_p (d_{amb}^3 M_p A)^{-1} (d_1^3 - d_0^3) \quad (11a),$$

for in-cloud conditions or

$$t_{CF} = \frac{3}{8} r_p (M_p A)^{-1} \ln \frac{d_1}{d_0} \quad (11b)$$

in a cloud-free environment ( $d_{amb} = 2 d_{dry}$ ). For these calculations, we assume that all  $\text{SO}_2$  is dissolved into solution and that the reactions are not oxidant limited. This assumption is more likely true in cloud and provides an upper limit to the time-scale of the processes involved.

## 2.8 Time in cloud

Most of the aerosol processing rates are sensitive to the presence of clouds, as a higher relative humidity increases the ambient particle diameter and some of the aerosol is activated into cloud droplets. As an estimation, it can be assumed that the ratio of the time in cloud  $t_c$  to the total observation time  $t_t$  is equal to the ratio of the volume filled with cloud to the total MBL volume.  $t_c$  can then be calculated after

$$t_c = t_t \times CCR \times \frac{h_{MBL} - h_{CB}}{h_{MBL}} \quad (12)$$

with  $h_{MBL}$  height of the subsidence inversion,  $h_{CB}$  height of cloud base and  $CCR$  ratio of cloud cover. As vertical velocities in cloud are usually higher than in cloud-free environment,  $t_c$  is slightly overestimated by Equation 12. To adjust for this overestimation in a crude manner, we arbitrarily chose to apply a  $\approx 25\%$  reduction to the value of  $t_c$  calculated by Equation 12 in both Lagrangian cases.

## 3. Case Studies

The time scale analysis case studies examine the evolution of fine and accumulation mode aerosol in the MBL during LAG1 and LAG2 over a period of approximately 26 hours. Mean dry diameters for fine and accumulation mode are derived from spectra measured during the Lagrangians. In order to calculate realistic timescales, hygroscopic growth of particles in high humidity conditions in and out of cloud must be accounted for. Out of cloud, a representative boundary layer humidity of 95% is used (Johnson et al. a, this issue). Measured growth factors for sub-micrometer particles during ACE-2 were between 1.6 and 1.8 at  $\text{RH} = 90\%$  (Swietlicki et al., this issue). Therefore the ambient cloud-free particle size is taken to be twice the dry diameter. In cloud, relative humidity is slightly higher than 100%, leading to activation of some particles into cloud droplets. For non-activated interstitial aerosol, maximum sizes are reached at the point of peak supersaturation in the cloud, and thereafter, as the parcel continues to rise, the particles

reduce slightly in size as supersaturation decreases with height. For non-activated interstitial sulphate aerosols, O'Dowd et al. (1999d) illustrated that the typical size reached is four times that of the particle dry size. Consequently, for treating aerosol interactions in cloud, a growth factor of 4 is assumed for interstitial particle size. All calculations are performed for 'ambient' RH, i.e. with ambient or in-cloud diameters, and respective coefficients are chosen accordingly. However, in order to avoid confusion, modes will still be referred to with their dry diameters.

The following sections only give a short overview over the experiments. An explicit description of synoptic conditions and measured MBL thermodynamics and microphysics evolution during the Lagrangians, details on instrumentation and measurement techniques and the C-130 flight patterns can be found in the general Lagrangian overview paper (Johnson et al. a, this issue) and the LAG1 and LAG2 overviews (Johnson et al. b, this issue, Osborne et al., this issue).

### 3.1 LAG1-Clean Marine Case

#### **Observations:**

In course of this experiment, three flights were carried out with the C-130 between July 3<sup>rd</sup> and 5<sup>th</sup>. A fourth flight was performed by the Pelican aircraft on July 5<sup>th</sup>, however, due to tracking-balloon failure, there is some doubt as to whether or not the Pelican sampled within the tagged air parcel. Consequently, data from this platform are not used. The dominant air mass was of polar origin with hardly any passage over the continent. Broken cumulus was observed during most of LAG1 (Johnson et al. a, this issue).

This study focuses on changes in aerosol number and size distribution in the surface layer over a 26 hours period starting at 00:30 hours on July 4<sup>th</sup>. During the first flight, Johnson et al. (b) (this issue) report a well-mixed surface layer, topped by a de-coupled cloud layer with cloud base at an altitude of  $\approx 600$  m. This structure is mirrored in the number concentration of the fine mode aerosol, measured by an ultrafine Condensation Particle Counter (CPC, lower cut-off diameter 3 nm, Johnson et al. b, this issue). This concentration was lower in the cloud layer than in the surface layer. The number concentration of the accumulation mode aerosol, derived from Passive Cavity Aerosol Spectrometer Probe (PCASP) measurements (Osborne et al., this issue) and covering  $d = 100$ -500 nm, showed no dependence on altitude during the whole period of observation. With the height of the subsidence inversion steadily decreasing, the surface layer grew until the whole MBL appeared to be well-mixed.

Figure 1 illustrates the main evolution of wind speed and MBL height during the first Lagrangian. The height of the subsidence inversion decreased from  $\approx 1500$  m to 800 m, causing a significant reduction of the total mixing volume. Wind speed data taken from the ECMWF model at the same time indicates changes in the surface layer wind speed from  $6 \text{ m s}^{-1}$  to  $15 \text{ m s}^{-1}$ , in close agreement with the observed wind speeds (Johnson et al. a, this issue). Time in cloud was calculated after Equation 12. The evolution of the MBL height was derived from a linear interpolation to the observed changes, while cloud base was assumed to be constant at 600 m. For the first third of the experiment, peak cloud droplet concentrations encountered were of the order of  $50$ - $60 \text{ cm}^{-3}$ , while towards the end of the experiment, peak concentrations were of ranged from  $120$ - $170 \text{ cm}^{-3}$ . The calculations were performed with a cloud cover ratio of  $3/8^{\text{th}}$ , which is somewhat lower than suggested by observations during the flights ( $\approx 4/8^{\text{th}}$ ), in order to account for the overestimation imposed by Equation 12. The overall time for the aerosol in cloud during the first Lagrangian is 4.6 hours.

Size distributions  $dN/d\log d$  of the aerosol in the surface mixed layer for start and end of the 26 hours are shown in Figure 2. The accumulation mode spectrum is derived from data of the C-130 PCASP. The fine mode spectrum is calculated from Differential Mobility Particle Sizer (DMPS) data measured on the R / V Vodyanitskij (Bates et al, this issue) and scaled to the total number of fine mode particles observed by the ultrafine CPC on the aircraft at start and end of LAG1, assuming the mean mode diameter of the fine mode to have remained constant over the period. This method to derive the fine mode spectrum was chosen, because no fine mode spectral data from the C-130 was available for LAG1. At the start of the experiment, the aerosol distribution was primarily bi-modal with a fine mode concentration of  $1050 \text{ cm}^{-3}$ , centred at  $d_{\text{dry}} = 30$  nm, and an accumulation mode concentration of  $76 \text{ cm}^{-3}$ , centred at  $d_{\text{dry}} = 220$  nm. By the end of the evolution experiment, the fine mode concentration reduced to  $750 \text{ cm}^{-3}$ , while the accumulation mode concentration increased to  $162 \text{ cm}^{-3}$ . These input values for the LAG1 case study are summarised in Table 1. The remaining fine mode particles are assumed to remain constant in size, the measured accumulation mode mean diameter however decreased to  $\approx 180$  nm. The observed changes suggest that (1) some of the fine mode particles grow into the accumulation mode and / or (2) there is a direct injection of new accumulation mode particles. The additional accumulation mode particles show a mode diameter smaller than the pre-existing mode.

**Time scale Analysis :**

The mean wind speed in the surface layer was  $8.7 \text{ m s}^{-1}$  for the first half of LAG1 and  $12.3 \text{ m s}^{-1}$  for the second half. Average dry deposition fluxes calculated after Equation 1 range from  $-0.44 \times 10^{-4} \text{ cm}^{-3} \text{ s}^{-1}$  to  $-0.99 \times 10^{-4} \text{ cm}^{-3} \text{ s}^{-1}$  for fine mode particles and  $-0.03 \times 10^{-4} \text{ cm}^{-3} \text{ s}^{-1}$  to  $-0.04 \times 10^{-4} \text{ cm}^{-3} \text{ s}^{-1}$  for accumulation mode particles. Total losses over 26 hours are  $-6 \text{ cm}^{-3}$  particles from the fine mode and  $-0.3 \text{ cm}^{-3}$  from the accumulation mode.

No precipitation was observed during the clean Lagrangian, precipitation scavenging as a loss mechanism can therefore be neglected.

The evolution of the MBL during LAG1 was dominated by a decrease in mixing volume. Therefore, mixing of MBL and tropospheric air on a large scale, as during LAG2, is unlikely to have occurred and no significant changes in MBL particle concentration due to dilution by tropospheric air are expected. Local entrainment, which took place at the subsidence inversion, is not considered here.

Sea-salt particle production is calculated after Equation 3. The production rate varies between  $+0.41 \times 10^{-4} \text{ cm}^{-3} \text{ s}^{-1}$  and  $+32 \times 10^{-4} \text{ cm}^{-3} \text{ s}^{-1}$  alongside with changes in both wind speed and MBL height. The net gain over 26 hours is  $+108 \text{ cm}^{-3}$  sea-salt particles, which are assumed to have accumulation mode sizes. This result is supported by analysis of sub-micrometer particle filter samples from the C-130, which show a significant (more than three-fold) increase in sea-salt particle mass during the course of LAG1 (Johnson et al. b, this issue), as well as by filter samples measured downwind at Hidalgo (Putaud et al., this issue).

To determine if diffusive coagulation of fine mode particles ( $d_{dry} = 30 \text{ nm}$ ) with those at the lower end of the accumulation mode ( $d_{dry} = 200 \text{ nm}$ ) can account for the enhancement of particles at the mid-to-higher end of this mode ( $d_{dry} = 250 \text{ nm}$ ), we perform the calculation, using Equation 5, for a concentration in this size range of  $40 \text{ cm}^{-3}$  (i.e. about half of the total accumulation mode concentration). The coagulation coefficient for ambient cloud-free conditions is  $K_{12} = 2.8 \times 10^{-8} \text{ cm}^3 \text{ s}^{-1}$  (Seinfeld and Pandis, 1997, for this and all other coagulation coefficients). A coagulation rate of  $-11 \times 10^{-4} \text{ cm}^{-3} \text{ s}^{-1}$  leads to total losses of  $-104 \text{ cm}^{-3}$  particles from the fine mode in 26 hours. The time to grow a particle from dry diameter 200 nm to 250 nm after Equation 6 is 111 days. The diffusive coagulation rate is increased to approximately  $-33 \times 10^{-4} \text{ cm}^{-3} \text{ s}^{-1}$  by the presence of a cloud droplet mode with  $d_2 = 15 \mu\text{m}$  and  $N_2 = 100 \text{ cm}^{-3}$  (Johnson et al. b, this issue) and a coagulation coefficient of  $K_{12} = 3.18 \times 10^{-8} \text{ cm}^3 \text{ s}^{-1}$ . The total loss of fine mode particles during 4.6 hours in cloud is  $-54 \text{ cm}^{-3}$ . A particle with  $d_{dry} = 200 \text{ nm}$ , activated to a  $15 \mu\text{m}$ -droplet, would need approximately 97 days to grow to 250 nm according to Equation 6. The loss rate due to self-coagulation of the fine mode after Equation 7 is  $-5 \times 10^{-4} \text{ cm}^{-3} \text{ s}^{-1}$ , using a  $K_{11}$  of  $0.97 \times 10^{-9} \text{ cm}^3 \text{ s}^{-1}$ .  $48 \text{ cm}^{-3}$  fine mode particles are removed in 26 hours. The time to grow one particle from dry diameter 30 nm to 250 nm by self-coagulation, calculated after Equation 6, is  $> 10^3$  days. The self-coagulation rate for the accumulation mode ( $d_{dry} = 250 \text{ nm}$ ) under the given conditions ( $K_{11} = 0.39 \times 10^{-9} \text{ cm}^3 \text{ s}^{-1}$ ) is  $-1.12 \times 10^{-6} \text{ cm}^{-3} \text{ s}^{-1}$ . This leads to a loss of one particle  $\text{cm}^{-3}$  in 26 hours. For self coagulation (coalescence) in cloud, the loss rate ( $K_{11} = 3.15 \times 10^{-9} \text{ cm}^3 \text{ s}^{-1}$ ) of particles is significantly less than  $1 \text{ cm}^{-3}$ .

During the clean Lagrangian,  $\text{SO}_2$ -mixing ratios between 6 and 44 ppt were measured (Johnson et al., b, this issue). Using a mean value of 20 ppt and assuming a hydroxyl concentration of  $[\text{OH}] = 10^6$  molecules per  $\text{cm}^3$ , a constant surface sink with  $d_s = 250 \text{ nm}$ ,  $N_s = 50 \text{ cm}^{-3}$ , and an accommodation coefficient  $a = 1$ , a steady state  $\text{H}_2\text{SO}_4$ -concentration of  $5.2 \times 10^{-2}$  ppt is achieved. This acid-concentration leads to a growth rate of  $+7.2 \times 10^{-5} \text{ nm s}^{-1}$  and a particle growth time of 35 days from diameter 30 nm to 250 nm.

Growth rates due to aqueous-phase sulphur production are calculated after Equation 10 and 11a, b. Typical concentrations of gas phase species during the clean Lagrangian were 20 ppt  $\text{SO}_2$ , 0.5 ppb  $\text{H}_2\text{O}_2$  and 30 ppb  $\text{O}_3$ . For a cloud-free environment, a growth rate of  $+10^{-9} \text{ nm s}^{-1}$  and an according growth time from the fine mode to the accumulation mode of the order of  $10^4$  days are found. The calculations were done assuming a pH of 3, which is already very high under the given conditions (Lin et al., 1992). The growth rate in cloud is  $+1.7 \text{ nm s}^{-1}$  for a mean cloud droplet diameter of  $15 \mu\text{m}$  and a pH of 6. The resulting growth time is 35 minutes, which is within the time the aerosol spent in cloud during the first Lagrangian.

**Dominating Processes**

Loss, gain and growth rates and changes in particle numbers for LAG1 are summarised in Table 2. The observed spectral changes can be explained by a combination of coagulation and an enhanced sea-salt flux into a reduced mixing volume. Diffusive coagulation is the dominant loss process for fine mode particles, removing  $54 \text{ cm}^{-3}$  particles in, and  $104 \text{ cm}^{-3}$  particles, out of cloud. Self-coagulation contributes with around  $-48 \text{ cm}^{-3}$  particles. Together, these three

processes are able to cover  $\approx 70$  % of the total observed fine mode losses of  $-300 \text{ cm}^{-3}$  particles. The increase in the accumulation mode by  $86 \text{ cm}^{-3}$  particles can be explained by production of sea-salt particles, which accounts for  $+108 \text{ cm}^{-3}$  particles under the given conditions. The only growth mechanism fast enough to fit into the timescale of the experiment is the growth of particles due to aqueous-phase chemical reactions in cloud droplets with a growth time of 35 min from the fine mode to the accumulation mode, however, time scale analysis of this processes possesses the greatest uncertainty due to the massively non-linear nature. This processes may contribute some particles to the accumulation mode, however, under given conditions the sea-salt flux is more than sufficient to explain the observations.

### 3.2 LAG2-Polluted Case

#### **Observations:**

The experiment included three flights by the C-130, carried out between July 16<sup>th</sup> and July 18<sup>th</sup>. The ECMWF back trajectories show a continental air mass from the north of France. Full stratocumulus cover was present during the whole period. A description of synoptic conditions and MBL evolution can be found in Johnson et al. (this issue). Osborne et al. (this issue) discuss details and results of all measurements performed on board the C-130 during LAG2.

The analysis covers 26 hours from 02:00 hours on July 17<sup>th</sup> to 06:00 hours on July 18<sup>th</sup>. The MBL was well-mixed at beginning and end of the experiment, although de-coupling occurred during daytime of the 17<sup>th</sup>. The aerosol showed some layer structure, especially a pollution layer above the subsidence inversion at the beginning of the first flight, however, the surface layer aerosol appeared mostly well-mixed (Osborne et al., this issue). Possible influences of both the de-coupling and the particle layers on the overall observed changes are excluded from this study, as their timescales were rather short compared to the total period. Figure 3 shows the evolution of MBL altitude and surface layer wind speed during LAG2. The height of the subsidence inversion increases from 500 m to 1100 m during the observed period. This suggests mixing of free tropospheric air into the MBL. The modelled surface layer wind speed decreases from  $10 \text{ m s}^{-1}$  to below  $8 \text{ m s}^{-1}$  during the first half of the 26 hours. After that it remains rather constant between  $8\text{-}9 \text{ m s}^{-1}$ . The depth of the cloud layer was  $\approx 150 \text{ m}$ . Additionally, cumuli were observed in the middle of the observation period. Peak cloud droplet concentration approached  $300 \text{ cm}^{-3}$  for the stratocumulus cloud encountered and  $400 \text{ cm}^{-3}$  for cumulus.

An estimation of the time in cloud after Equation 12 with a constant stratocumulus depth  $h_{\text{MBL}} - h_{\text{CB}} = 150 \text{ m}$  and  $\text{CCR} = 1$  results in  $t_c = 4$  hours, which is somewhat shorter than the 6.5 hours estimated by Osborne et al.. Figure 4 shows particle size distributions  $dN / d\log d$  for begin and end of the 26 hour period, measured by a Scanning Mobility Particle Sizer (SMPS) and Active Scattering Aerosol Spectrometer Probe (ASASP-X) on board the C-130 (Johnson et al. a, this issue). The aerosol size distribution during the start of this experiment was bi-modal with a fine mode at  $d_{\text{dry}} = 60 \text{ nm}$ ,  $N = 2700 \text{ cm}^{-3}$  and an accumulation mode at  $d_{\text{dry}} = 100 \text{ nm}$ ,  $N = 670 \text{ cm}^{-3}$ . By the end of the experiment there was no change in modal diameter in either the fine or the accumulation mode, concentrations however were observed to decrease significantly in both modes. The fine mode concentration fell to  $1150 \text{ cm}^{-3}$ , the accumulation mode concentration to  $430 \text{ cm}^{-3}$ . The input parameters for the LAG2 analysis are listed in Table 1. The lack of apparent increase in mean mode diameter suggests that either no growth processes were occurring over the given time scale or the size distribution is self-preserving in size. The loss of concentration observed in both modes suggests a significant removal processes occurring over the period.

#### **Time scale analysis**

As variations in wind speed during the polluted Lagrangian were not as large as during LAG1, dry deposition fluxes were derived for an average wind speed  $u = 8.4 \text{ m s}^{-1}$  for the whole 26 hours. Mean fluxes are between  $-1.45 \times 10^{-4} \text{ cm}^{-3} \text{ s}^{-1}$  and  $-0.99 \times 10^{-4} \text{ cm}^{-3} \text{ s}^{-1}$  for the fine mode and  $-0.51 \times 10^{-4} \text{ cm}^{-3} \text{ s}^{-1}$  and  $-0.34 \times 10^{-4} \text{ cm}^{-3} \text{ s}^{-1}$  for the accumulation mode, resulting in total losses of  $-11 \text{ cm}^{-3}$  fine mode particles and  $-4 \text{ cm}^{-3}$  accumulation mode particles, respectively.

Drizzle was reported during two flights of LAG2. Drizzle drops reached the ground only during the first observation (Osborne et al.). Scavenging rates were calculated after Equation 2 for an assumed rain drop diameter  $d_{\text{drop}} = 0.4 \text{ mm}$ . Numerically derived values for ambient  $L_n$  were taken from Seinfeld and Pandis (1997). They are  $L_n \approx 8.3 \times 10^{-6} \text{ s}^{-1}$  for scavenging of particles with  $d_{\text{dry}} = 60 \text{ nm}$  and  $L_n \approx 2.5 \times 10^{-6} \text{ s}^{-1}$  for  $d_{\text{dry}} = 200 \text{ nm}$ . Resulting scavenging rates are  $-224 \times 10^{-4} \text{ cm}^{-3} \text{ s}^{-1}$  to  $-213 \times 10^{-4} \text{ cm}^{-3} \text{ s}^{-1}$  for fine mode particles and  $-16 \times 10^{-4} \text{ cm}^{-3} \text{ s}^{-1}$  for accumulation mode particles. Assuming 2 hours of precipitation, the total losses are  $-158 \text{ cm}^{-3}$  particles from the fine mode and  $-12 \text{ cm}^{-3}$  particles from the accumulation mode. These numbers agree well with results from Osborne et al., who estimate about 8 % of the aerosol number is removed per day at the observed precipitation rate.

Production rates for sea-salt particles were calculated after Equation 6, using the wind speed evolution shown in Figure 3. Values for the production rate range from  $+0.63 \times 10^{-4} \text{ cm}^{-3} \text{ s}^{-1}$  to  $+2.2 \times 10^{-4} \text{ cm}^{-3} \text{ s}^{-1}$ , a total of  $+11 \text{ cm}^{-3}$  accumulation particles is gained over 26 hours.

A significant increase in MBL-volume during LAG2 is indicated in Figure 3. Particle numbers in the free troposphere were usually lower than in the MBL, except for a short interval at the beginning of the first flight, when a polluted layer was observed above the subsidence inversion. Neglecting this pollution, the mixing process induced by the change in volume had to reduce the particle concentration in the MBL. Concentrations  $N_M$  at the end of the 26 hour interval are calculated after Equation 4 with an initial MBL-height of 500 m, a change in altitude of +600 m and free tropospheric particle concentrations of  $1000 \text{ cm}^{-3}$  in the fine mode and  $200 \text{ cm}^{-3}$  in the accumulation mode. Reductions due to the mixing are  $-1145 \text{ cm}^{-3}$  fine mode particles and  $-285 \text{ cm}^{-3}$  accumulation mode particles.

As in LAG1, we explore the growth timescale for particles at the lower end of the accumulation mode sizes ( $d_{dry} = 150 \text{ nm}$ ) to grow into sizes in the mid-to-higher end of the accumulation mode ( $d_{dry} = 200 \text{ nm}$ ) by diffusive coagulation with fine mode particles ( $d_{dry} = 60 \text{ nm}$ ). Since there is approximately one third of the accumulation mode particles occupying the lower size of the mode, we calculate the coagulation coefficient for a concentration of  $N = 200 \text{ cm}^{-3}$  in this size range. Using a coagulation coefficient of  $K_{12} = 1.1 \times 10^{-9} \text{ cm}^3 \text{ s}^{-1}$ , and taking account of the concentrations in both the fine mode and the sub-set of the accumulation mode, a coagulation rate of  $-5.9 \times 10^{-4} \text{ cm}^{-3} \text{ s}^{-1}$  is derived from Equation 5, leading to a total loss of  $-55 \text{ cm}^{-3}$  particles in 26 hours. Equation 6 gives a time of 83 days for a particle to grow from  $d_{dry} = 150 \text{ nm}$  to  $200 \text{ nm}$  by this process. Coagulation with cloud droplets is calculated for a cloud droplet mode with  $d_2 = 14 \mu\text{m}$ ,  $N_2 = 250 \text{ cm}^{-3}$  (Osborne et al., this issue). With a coagulation coefficient  $K_{12} = 2.6 \times 10^{-8} \text{ cm}^3 \text{ s}^{-1}$ , Equation 5 delivers a mean loss rate of  $-167 \times 10^{-4} \text{ cm}^{-3} \text{ s}^{-1}$  for the fine mode. During 4 hours in cloud,  $241 \text{ cm}^{-3}$  fine mode particles are thus removed. The growth time for an activated sub-accumulation mode particle to  $200 \text{ nm}$  after Equation 6 is 5.7 days. The ambient self-coagulation coefficient for particles with  $d_{dry} = 60 \text{ nm}$  is  $6.8 \times 10^{-10} \text{ cm}^3 \text{ s}^{-1}$ , the resulting self-coagulation rate for the fine mode after Equation 7 is  $-23 \times 10^{-4} \text{ cm}^{-3} \text{ s}^{-1}$ .  $215 \text{ cm}^{-3}$  particles would therefore be removed over 26 hours. Equation 6 gives a time of 227 days to grow a particle from the fine to the accumulation mode by self-coagulation. Self-coagulation in the accumulation mode after Equation 7 delivers a loss rate of  $-0.88 \times 10^{-4} \text{ cm}^{-3} \text{ s}^{-1}$  and total losses of  $-8 \text{ cm}^{-3}$  particles, using a  $K_{11}$  of  $4 \times 10^{-10} \text{ cm}^3 \text{ s}^{-1}$ . As in LAG1, self-coagulation of cloud droplets leads to a loss of less than  $1 \text{ cm}^{-3}$  over the period.

$\text{SO}_2$ -concentrations changed significantly during LAG2 (Osborne et al., this issue), with maximum values close to 800 ppt in the early hours of July 17<sup>th</sup>, which later decreased to  $< 100$  ppt. A mean  $\text{SO}_2$ -concentration of  $\text{SO}_2$  of 125 ppt was used for the time-scale calculation. The surface sink for  $\text{SO}_2$  was assumed to be the accumulation mode with  $d_{dry} = 200 \text{ nm}$  and a mean concentration of  $500 \text{ cm}^{-3}$ . Applying Equation 8, 125 ppt  $\text{SO}_2$  yield a steady-state  $\text{H}_2\text{SO}_4$  - concentration of 0.3 ppt. The resulting condensation growth rate for a particle after Equation 9 is  $+0.5 \times 10^{-4} \text{ nm s}^{-1}$ , the growth time from fine mode to accumulation mode 35 days. Performing the same calculation for a  $\text{SO}_2$  mixing ratio of 750 ppt over 26 hours results in a growth time of 5 days.

Growth rates and times for aqueous-phase oxidation reactions after Equations 10 and 11a, b are calculated for  $[\text{SO}_2] = 125$  ppt, mixing ratios for  $\text{O}_3$  and  $\text{H}_2\text{O}_2$  are equal to LAG1. In cloud-free environment, a growth rate of  $+7.0 \times 10^{-6} \text{ nm s}^{-1}$  results in a growth time from fine mode to accumulation mode of  $10^3$  days. In cloud, assuming a fraction of particles activated to cloud droplets with diameter  $14 \mu\text{m}$ , a growth rate of  $+2.64 \text{ nm s}^{-1}$  leads to a growth time of 2.3 minutes.

#### **Dominant Processes:**

The results of the time-scale analysis for LAG2 are summarised in Table 3. The dominant mechanism is mixing of MBL and tropospheric air, which reduces particle concentrations in the fine mode by  $-1145 \text{ cm}^{-3}$ . in fine and  $-285 \text{ cm}^{-3}$  in the accumulation mode. Coagulation, accounting for total losses of  $-511 \text{ cm}^{-3}$ , and precipitation scavenging with losses of  $-158 \text{ cm}^{-3}$ , provide additional sinks for fine mode particles. The accumulation mode concentration is reduced by  $-285 \text{ cm}^{-3}$  due to the mixing. In comparison, all other processes influencing this mode, i. e. sea-salt production, are negligible. The observed reductions in number concentration of  $-1200 \text{ cm}^{-3}$  in the fine mode and  $-240 \text{ cm}^{-3}$  in the accumulation mode can be sufficiently explained by mixing and coagulation, although aqueous phase time scales suggest there should be some growth from the fine mode to the accumulation mode. The net overestimation of losses may be caused by the fact that the mixing in of air from the elevated pollution layer at the beginning of the experiment, which increased the number of particles in both modes (Osborne et al., this issue), was neglected in this study. It is interesting to note that in-cloud diffusive coagulation losses for the fine mode are higher relative to diffusive coagulation out of cloud during LAG2 whereas they are lower in LAG1. This primarily results from the non-linear

relationship between coagulation coefficients as a function of size. For LAG1, the difference in coagulation coefficients for the converted wet sizes in and out of cloud (60nm and 120nm) is significantly larger than the difference encountered in LAG2 (120 nm and 240 nm). Consequently, the smaller the fine mode is, the more likely that diffusive coagulation out of cloud will dominate over that in cloud.

#### 4. Discussion

Fully integrated meteorological and process aerosol-cloud-chemistry models are computationally demanding. It is therefore useful to determine what processes can either be eliminated, included explicitly, or parameterised in large scale models. The purpose of this time-scale analysis is essentially to highlight, which processes should receive the greatest attention regarding inclusion of full micro-physical or chemical components. Consequently, a high degree of accuracy is not to be expected, particularly as processes are treated as individual rather than as interacting. Nevertheless, the range of errors associated with the variance in the most sensitive inputs to each calculation for the dominant processes should be examined. Four dominant processes emerge from the timescale analysis: (1) coagulation as a loss mechanism of fine mode particles; (2) sea-salt production, (3) entrainment as an exchange process; and (4) in-cloud chemical processing as a growth mechanism.

For the self-coagulation analysis, the most sensitive input parameter is the mode diameter used. Increasing the initial  $d_{dry}$  by 20 % results in less than a 7 % decrease in loss rates for both Lagrangians, while decreasing it by 20 % results in a maximum of 12 % over-estimate in loss rates. For diffusive coagulation out of cloud, increasing  $d_{dry}$  by 20% decreases losses by 27% in LAG1 and 2 % in LAG2. Decreasing the initial size by 20 % leads to an over-prediction in losses of 27 % in LAG1 and 9 % in LAG2. For diffusive coagulation in cloud, increasing  $d_{dry}$  by 20% decreased the losses by 4% while decreasing  $d_{dry}$  by 20% results in a 7% enhancement in calculated losses.

For the production of sea-salt, allowing a -20 % error in the source rates results in a 33 % reduction in the predicted sea-salt concentration, while allowing a +20% error in the source rates leads to a 74 % enhancement in the predicted concentration during LAG1. For LAG2, the under-prediction is 6 % while the over-prediction is 14 % for the same range of error.

The treatment of entrainment rates is quite difficult and prone to error as accurate measurements of entrainment rates are difficult to achieve. In LAG1, small scale entrainment at the FT-MBL interface was neglected, while in LAG2, this entrainment was assumed to be incorporated into the rapid increase in inversion height, and minimal in terms of mixing volume exchange after the rapid increase occurs. While the latter assumption is likely to be correct for LAG2, as the rate of increase in mixing height is larger than the calculated entrainment rate (Sollazzo et al., this issue), the former assumption is unlikely to be true for LAG1, since, even though the subsidence inversion is decreasing, entrainment is still ongoing. In an attempt to examine the influence local entrainment processes for LAG1, the derived entrainment rate ( $0.013 \text{ m s}^{-1}$ ) for LAG1 given by Sollazzo et al., (this issue) is used to examine the effect of this exchange of FT aerosol on the MBL concentrations. Inclusion of this entrainment processes is found to result in 25 % loss of fine mode particles and 15 % loss of accumulation mode particles over the period. These results lead to an over-estimation of particle loss when all processes are accounted for, particularly in the fine mode, however, there is considerable error associated with the techniques used to derived entrainment rates by Sollazzo et al. (this issue). Although it was assumed that the boundary layer is always well mixed, this was not always the case as for some periods during each Lagrangian, as the boundary layer was sometimes decoupled. Nevertheless, significant mixing and exchange between the surface layer and the decoupled cloud layer will most likely have occurred due to the presence of cumulus clouds. The mixing rate between the de-coupled cumulus and surface layer is obviously significantly greater (illustrated only partially by the cloud volume at any given time) than that encountered between the cumulus layer and the free troposphere. Consequently, de-coupling of the boundary layer, in the presence of significant cumulus fields, will have little impact on the general boundary layer aerosol dilution / enhancement by entrainment at the free troposphere interface.

By far, the most non-linear and least suitable process for timescale analysis, is the aqueous phase chemistry in cloud droplets.  $\text{SO}_2$  oxidation in the aqueous phase is highly dependent on solution pH, however, this pH is not only massively variable with particle composition, it is also massively variable with particle size which can change rapidly, particularly in cloud (O'Dowd et al., 1999d). While the timescale arguments given here suggest that particle growth can occur rapidly through  $\text{SO}_2$  oxidation in cloud droplets, this calculation is conducted for a single particle size and using very much idealised solution chemistry. For low  $\text{SO}_2$ -concentrations, O'Dowd et al., (1999d) have shown that use of ideal chemical solution effects can overestimate the amount of oxidation occurring by more than 100 % when compared to that of the robust Pitzer treatment of non-ideal solution effects. The error is even greater when mass transport limitations are ignored. Additionally, they also illustrate that, in the presence of high sea-salt and low sulphate aerosol

concentrations, similar to that encountered in LAG1, as much as 90 % of SO<sub>2</sub> oxidation occurs in droplets activated on sea-salt nuclei. The growth of sulphate aerosol from in-cloud oxidation processes is therefore a strong function of not only SO<sub>2</sub>, O<sub>3</sub> and H<sub>2</sub>O<sub>2</sub>, but also of sea-salt aerosol concentration (O'Dowd et al., 1999b). Consequently, given the low SO<sub>2</sub> and high sea-salt concentrations encountered on LAG1, it is most likely that the vast majority of SO<sub>2</sub>-sulphate conversion occurred in sea-salt nuclei, leaving little SO<sub>2</sub> available for growing sulphate nuclei significantly.

In LAG2, coinciding with high wind speeds, SO<sub>2</sub> concentrations rapidly fell from 800 ppt to about 100 ppt at the very beginning of the experiment. Thus, it is likely that the majority of the SO<sub>2</sub> was depleted to sea-salt aerosols. Total sulphate production in sulphate based nuclei is independent of sulphate nuclei concentration (O'Dowd et al., 1999d) since, if the number of sulphate based droplets is increased, the solution ionic strength increases, pH reduces and the sulphate production per individual particle is also decreased. Consequently, for polluted clouds with high concentrations of sulphate based nuclei, particularly in the presence of sea-salt nuclei, any noticeable increase in sulphate particle size will be difficult to detect. Lack of growth in LAG2 suggests that chemical cloud processing during this experiment was negligible, most likely because the aerosol had reached thermodynamic and chemical equilibrium with respect to SO<sub>2</sub> oxidation.

Finally, we should note that we have ignored the role of organic aerosol formation in this analysis as it is unlikely to dominate the total aerosol mass when compared to the combined sea-salt and sulphate contributions. Organics are most likely to accelerate condensation growth processes, if resulting from gas-to-particle conversion processes, and be internally linked with sea-salt if mechanically produced. Putaud et al., (this issue) report average sub-micron organic carbon mass contributions of 25 %, relative to 56 % for combined sea-salt, ammonium and sulphate, for clean marine air and 11 %, relative to 74 % from sea-salt, ammonium and sulphate, for polluted air. Consequently, it is unlikely that the omission of organic aerosol will significantly affect the results reported here.

## 5. Conclusions

During LAG1, the aerosol evolution in a clean MBL under cloudy conditions was studied. The fine mode, centred at 30 nm, was observed to decrease in concentration from 1050 cm<sup>-3</sup>, to 750 cm<sup>-3</sup>, while the accumulation mode concentrations increased from 76 cm<sup>-3</sup> to 162 cm<sup>-3</sup>. Physical processes, particularly coagulation losses in the fine mode, and sea-salt production of accumulation mode particles at the ocean surface can explain the observed spectral changes. In LAG2, under polluted conditions, the fine mode with  $d_{dry} = 60$  nm, decreased from 2700 cm<sup>-3</sup> to 1150 cm<sup>-3</sup> while the accumulation mode concentration ( $d_{dry} = 200$  nm) decreased from 670 cm<sup>-3</sup> to 430 cm<sup>-3</sup>. No growth in either mode was observed and the reduction in concentration is explicable by dilution with cleaner, free tropospheric air as the mixing layer deepened. In both experiments, despite significant cloud cover, there was little or no evidence for chemical processing by clouds as previously observed by Hoppel et al. (1996) and O'Dowd et al. (1999c) over much shorter timescales. This suggests that, in this case, the ability for the existing aerosol to remove trace gases was very much diminished. Meteorology and physical aerosol interactions had the greatest influence on shaping the aerosol size distribution during these studies.

## Acknowledgements

This research is a contribution to the International Global Atmospheric Chemistry (IGAC) Core project of the International Geosphere-Biosphere Programme (IGBP) and is part of the IGAC Aerosol Characterisation Experiments (ACE). It has been supported by the European Union under contract ENV4-CT95-0032 (ACE2 LAGRANGIAN) and ENV4-CT97-0526 (PARFORCE).

## References

- Atkinson, R., D. L. Baulch, R. F. Cox, J. A. Kerr and J. Troe (1989). Evaluated kinetic and photochemical data for atmospheric chemistry: supplement III IUPAC subcommittee on gas kinetic data evaluation for atmospheric chemistry. *J. Phys. Chem. Ref. Data*, **18**, 881-1097.
- Bates, T., S., P. K. Quinn, D.S. Covert, D. J. Coffman, J. E. Johnson and A. Wiedensohler (2000). Aerosol Physical Properties and Controlling Processes in the Lower Marine Boundary Layer: A Comparison of Sub-Micron Data from ACE 1 and ACE 2. *Tellus*, this issue.
- Blanchard, D.C. (1980). The production, concentration and vertical distribution of the sea-salt aerosol. *Annales of the New York Academy of Science*, **338**, 330-347.
- Durkee, P, Johnson, D. W. , R. N. Ferek, T. Garrett, P. V. Hobbs, J Hudson, K. J. Noone, L. M. Russell, S. Platnick, J. P. Taylor, C. D. O'Dowd, W. Hooper, P. Durkee, K. Nielson, A. Ackerman, C. Bretherton, G. Innis, Y. Kogan, R. Flagan, J. Seinfeld, M. H. Smith, W. A.. Hoppel (1999). The impact of ship produced aerosols on the micro-physical characteristics of warm stratocumulus clouds: A test of Hypotheses 1.1a and 1.1b. *J. Atmos. Sci.*, in press.
- Hoppel W.A., G. M. Frick and R. E. Larson (1986). Effect of non-precipitating clouds on the aerosol size distribution in the marine boundary layer. *Geophys. Res. Letts.* ,**13**, 125-128.
- Hoppel, W. A., J. W. Fitzgerald, G. M. Frick and R. E. Larson (1990). Aerosol size distributions and optical properties found in the marine boundary layer over the Atlantic Ocean. *J. Geophys. Res.*, **95**, 3659-3686.
- Hoppel, W.A., G.M. Frick and J.W. Fitzgerald (1994). Marine boundary layer measurements of new particle formation and the effects non-precipitating clouds have on aerosol size distribution. *J. Geophys. Res.*, **99**, 14,443-14,459.
- IPCC, Intergovernmental Panel on Climate Change. Climate Change 1995, (1995). Cambridge University Press.
- Johnson, D. W., S. R. Osborne, R. Wood, K. Suhre, M. O. Andreae, R. Johnson, S. Businger, P. K. Quinn, T. Bates, P. Durkee, H. Johnson, L. M. Russell, K. Noone, P. Glantz, B. Bandy, C. O'Dowd, S. Rapsomanikis and J. Rudolph (2000a). An overview of the Lagrangian experiments undertaken during the North Atlantic Regional Aerosol Characterisation Experiment (ACE-2). *Tellus*, this issue.
- Johnson, D., W., S. Osborne, R. Wood, K. Suhre, P. Quinn, T. Bates, M. Andreae, K. Noone, P. Glantz, B. Bandy, J. Rudolph and C. O'Dowd (2000b). Observations of the Evolution of the Aerosol, Cloud and Boundary Layer Characteristics during the first ACE-2 Lagrangian Experiment. *Tellus*, this issue.
- Lin, X., W. L. Chameides, C. S. Kiang, A. W. Stelton and H. Berresheim (1992). A Model Study of the Formation of Cloud Condensation Nuclei in Remote Marine Areas. *J. Geophys. Res.*, **97**, 18161-18171.
- Murphy, D. M., J. R. Anderson, P. K. Quinn, L. M. McInnes, F. J. Brechtel, S. M. Kreidenweis, A. M. Middlebrook, M. Posfai, D. S. Thomson, and P. R. Buseck (1997). Sea-salt particles and aerosol radiative properties in the Southern Ocean marine boundary layer. *Nature* .
- Nicholls, S. and J. R. Leighton (1986). An observational study of the structure of stratiform cloud sheets. Part I: Structure. *Q. J. Roy. Met. Soc.*, **112**, 431-460.
- Nilsson, E. D., U. Rannik, E. Swietlicki, P. P. Aalto, J. Zhou and C. Leck (1998). Turbulent Aerosol Number Fluxes Over Sea And Pack Ice: Deposition And Wind Driven Fluxes Of Sub Micrometer Aerosol. *J. Aerosol Sci.*, **29**, Suppl. 1, S505-S506.
- O'Dowd, C. and M. H. Smith (1993). Physicochemical Properties of Aerosols over the Northeast Atlantic: Evidence for Wind-Speed Related Submicron Sea-Salt Aerosol Production. *J. Geophys. Res.*, **98**, 1137-1149.
- O'Dowd, C. D., M. H. Smith, I. E. Consterdine, and J. A. Lowe (1996). Marine aerosol, sea-salt, and the marine sulphur cycle - a short review. *Atmos Environ*, **31**, 73-80, 1997
- O'Dowd, C.D., J. Lowe, M.H. Smith and A.D. Kaye (1999a). The relative importance of sea-salt and nss-sulphate aerosol to the marine CCN population: An improved multi-component aerosol-droplet parameterisation. *Q. J. Roy. Met. Soc.*, Vol. 125, No. 556, 1295-1313.
- O'Dowd, C. D., J. A. Lowe, and M. H. Smith (1999b). Coupling sea-salt and sulphate interactions and its impact on predicting cloud droplet concentrations. *Geophys. Res. Letts.*, Vol. 26, No. 9, 1311-1314.
- O'Dowd, C. D., J.A. Lowe, and M.H. Smith (1999c). Observations and modelling of aerosol growth in marine stratocumulus-Case Study. *Atmos. Environ*, Vol. 33, issue 18, 3053-3062.
- O'Dowd, C. D., J.A. Lowe, N. Clegg, S.L. Clegg and M.H. Smith (1999d). Modelling heterogeneous sulphate production in maritime stratiform clouds. *J. Geophys. Res.* In press.
- Osborne, S. R., D. W. Johnson, R. Wood, B. J. Bandy, M. O. Andreae, C. D. O'Dowd, P. Glantz and K. Noone (2000). Observations of the evolution of the aerosol, cloud and boundary layer dynamic and thermodynamic characteristics during the second Lagrangian experiment of ACE-2. *Tellus*, this issue.
- Putaud, J.P., R. Van Dingenen, M. Mangoni, A. Virkkula, F. Raes, H. Maring, J.M. Prospero, E. Swietlicki, O.H. Berg, R. Hillamo and T. Makela (2000). Chemical mass closure and origin assessment of the submicron aerosol in the marine boundary layer and the free troposphere at Tenerife during ACE-2. *Tellus*, this issue.

- Raes, F. (1995). Entrainment of free tropospheric aerosols as a regulating mechanism for cloud condensation nuclei in the remote marine boundary layer. *J. Geophys. Res.*, **100** (D2), 2893-2903.
- Raes, F., T. Bates, G. Verver, D. Vogelenzang and M. Van Liedekerke (2000). The second aerosol characterisation experiment (ACE-2): Introduction, meteorological overview and main results. *Tellus*, this issues.
- Schwartz, S. E. (1986). Mass transport considerations pertinent to aqueous – phase reactions of gases in liquid-water clouds. In: *Chemistry of Multiphase Atmospheric Systems*. W. Jaeschke (ed.). Springer Verlag, Berlin, 415-471.
- Seinfeld, J. H. and S. N. Pandis (1997). *Atmospheric Chemistry and Physics*. John Wiley & Sons, New York.
- Sievering, H., J. Boatman, J. Galloway, W. Keane, Y. Kim, M. Luria, and J. Ray (1992). Removal of sulphur from the marine boundary layer by ozone oxidation in sea-salt aerosols. *Nature*, **360**, 571-573.
- Slinn, W. G. N., L. Hasse, B. B. Hicks, A. W. Hogan, D. Lai, P. S. Liss, K. O. Munnich, G. A. Sehmel and O. Vittori (1978). Some aspects of the transfer of atmospheric trace constituents past the air-sea interface. *Atmos. Environ.*, **12**, 2055-2087.
- Slingo, A. (1990). Sensitivity of the Earth's radiation budget to changes in low clouds. *Nature*, **343**, 49-51.
- Smith, M. H., P. M. Park and I. E. Consterdine (1990). North Atlantic Aerosol Remote Concentrations Measured at a Hebridean Coastal Site. *Atmos. Environ.*, **25A**, 547-555.
- Sollazzo, M. J, L. M. Russell, D. Percival, S. Osborne, R. Wood and D. W. Johnson (2000). Entrainment rates during ACE-2 Lagrangian experiments calculated from aircraft measurements. *Tellus*, this issue.
- Swietlicki, E., J. Zhou, D.S. Covert, K. Hameri, B. Busch, M. Vakeva, U. Dusek, O.H. Berg, A. Wiedensohler, P. Aalto, J. Makela, B.G. Marinsson, G. Papaspiropoulos, B. Mentes, G. Frank and F. Stratmann (2000). Hygroscopic properties of aerosol particles in the north-eastern Atlantic during ACE-2. *Tellus*, this issue.
- Wood, R., D. Johnson, S. Osborne, B. Bandy, M. Andreae, C. O'Dowd, P. Glantz and K. Noone (2000). Boundary layer, aerosol and chemical evolution during the third Lagrangian experiment of ACE-2. *Tellus*, this issue.

#### Figure Captions

**Figure 1** Evolution of the MBL during LAG1 after Johnson et al. b (this issue). Plotted are height of the subsidence inversion (triangles), height of cloud base (dotted line) and surface layer wind speed (diamonds). Wind speed is derived from the ECMWF model. Time 0 denotes the start of the period covered by the time-scale analysis.

**Figure 2** Particle size distribution in the surface layer at start (open symbols) and end (filled symbols) of LAG1.

**Figure 3** Evolution of the MBL during LAG2 (Osborne et al., this issue). Shown are the height of the subsidence inversion (triangles) and the wind speed in the surface layer (diamonds), derived from the ECMWF model. Time 0 is the start of the period covered in the time-scale analysis.

**Figure 4** Surface layer particle size distributions at start (open symbols) and end (filled symbols) of LAG2.

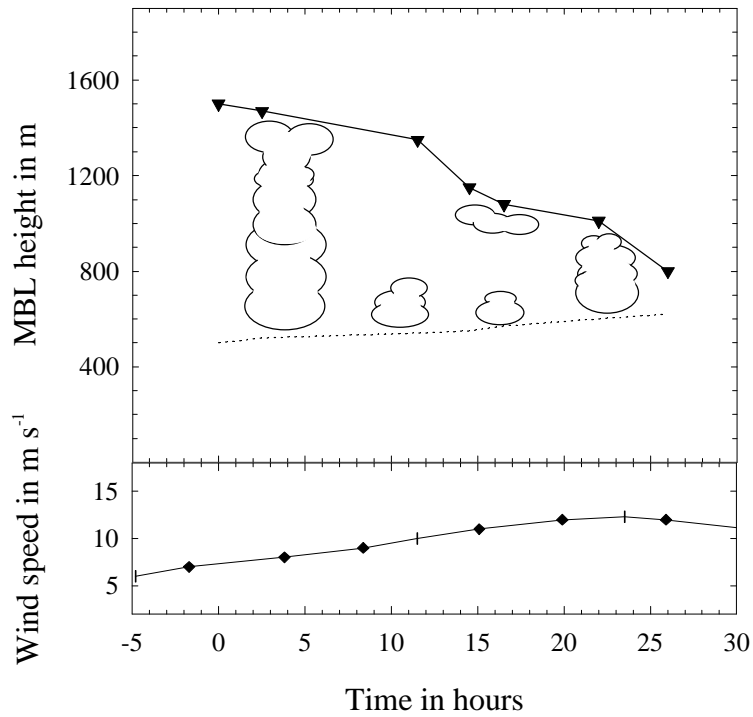


**Figure 1** Evolution of the MBL during LAG1 after Johnson et al. b (this issue). Plotted are height of the subsidence inversion (triangles), height of cloud base (dotted line) and surface layer wind speed (diamonds). Wind speed is derived from the ECMWF model. Time 0 denotes the start of the period covered by the time-scale analysis.

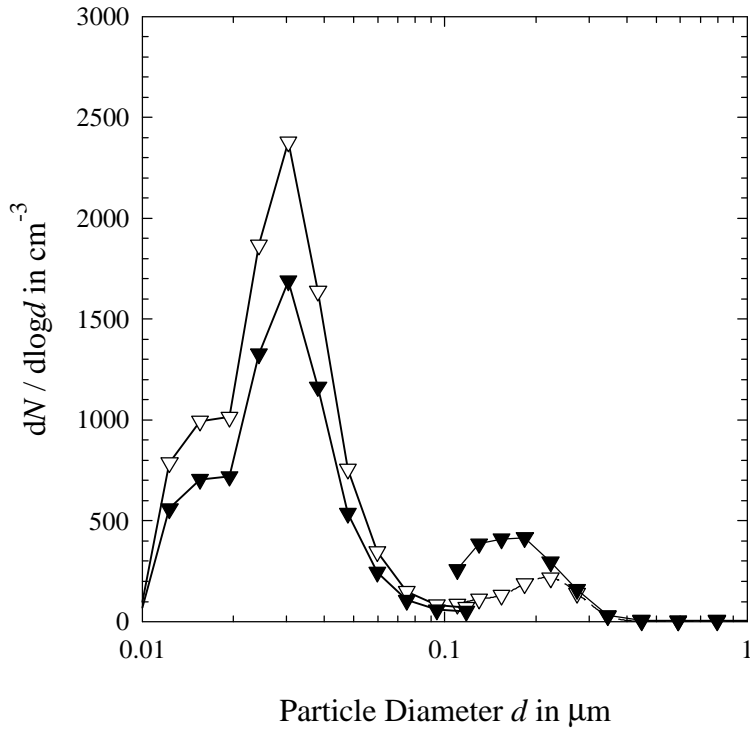


**Figure 2** Particle size distribution in the surface layer at start (open symbols) and end (filled symbols) of LAG1.

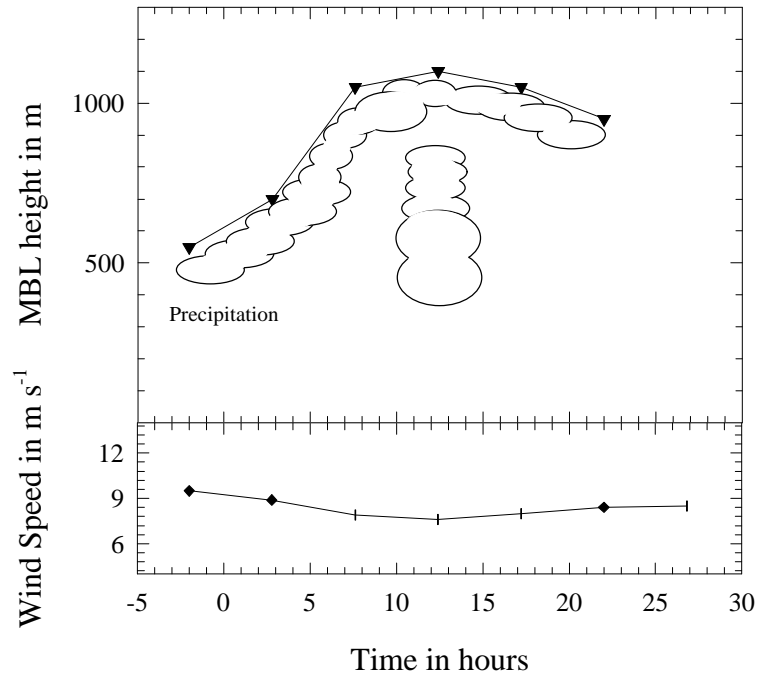


**Figure 3** Evolution of the MBL during LAG2 (Osborne et al., this issue). Shown are the height of the subsidence inversion (triangles) and the wind speed in the surface layer (diamonds), derived from the ECMWF model. Time 0 is the start of the period covered in the time-scale analysis.

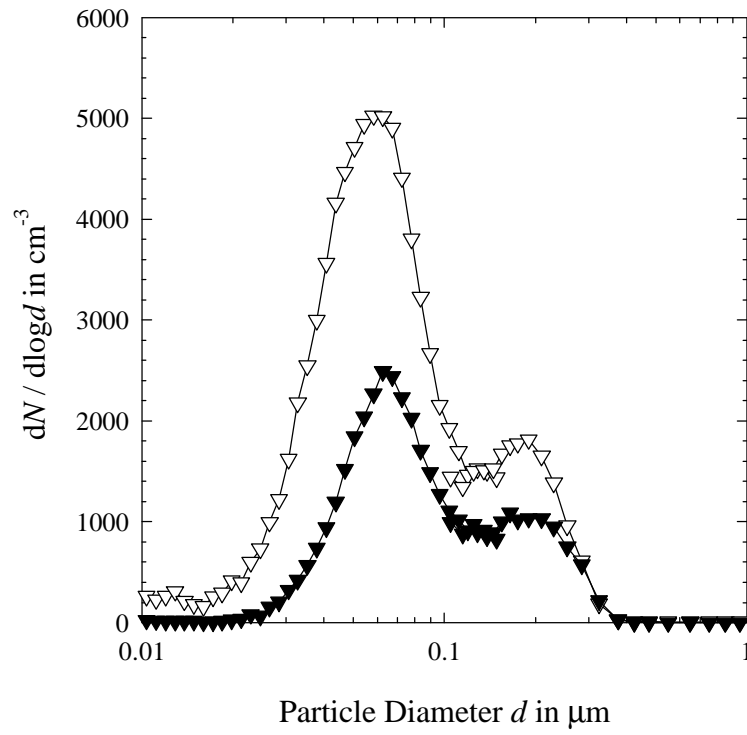


**Figure 4** Surface layer particle size distributions at start (open symbols) and end (filled symbols) of LAG2.

## Tables

**Table 1** Particle number concentrations per  $\text{cm}^3$  and dry mode diameters of fine and accumulation mode in the surface layer at start and end of LAG1 and LAG2, used as input parameters for the time scale analysis.

**Table 2** Results of the time scale analysis for the clean case (LAG1). Loss- and gain rates are given as maximum / minimum value over the observed period.

**Table 3** Results of the time scale analysis for the polluted case (LAG2). Loss- and gain rates are maximum / minimum values over 26 hours.

LAG1 - Clean case Particle concentration [cm <sup>-3</sup> ]			LAG2 - Polluted case Particle concentration [cm <sup>-3</sup> ]		
	Start	End		Start	End
<b>Fine mode</b> <i>d<sub>dry</sub></i> = 30 nm	1050	750	<b>Fine mode</b> <i>D<sub>dry</sub></i> = 60 nm	2700	1150
<b>Accumulation mode</b> <i>d<sub>dry</sub></i> = 250 nm	76	162	<b>Accumulation mode</b> <i>D<sub>dry</sub></i> = 200 nm	670	430

**Table 1** Particle number concentrations per cm<sup>3</sup> and dry mode diameters of fine and accumulation mode in the surface layer at start and end of LAG1 and LAG2, used as input parameters for the time scale analysis.

Process	Loss- / gain rates $dN / dt$ [ $1e-4 \text{ cm}^{-3} \text{ s}^{-1}$ ]	Total contribution in 26 hours [particles per $\text{cm}^3$ ]	Growth rates $dd / dt$ [ $\text{nm s}^{-1}$ ]	Growth time from $d_1$ to $d_2$
<b>Dry deposition</b>				
fine mode	-0.99 / -0.44	-6		
accumulation mode	-0.04 / -0.03	-0.3		
<b>Sea-salt production</b>	+0.41 / +32	+108		
<b>Diffusive coagulation of the fine mode</b>				
cloud-free	-12 / -11	-104		111 days (200 to 250 nm)
in cloud	-33 / -32	-54 (4.6 hrs in cloud)		97 days (200 to 250 nm)
<b>Self-coagulation</b>				
fine mode	-5.3 / -4.9	-48		$10^3$ days (30 to 250 nm)
accumulation mode	-0.01	-1		
<b>Condensation</b>			+7.2e-5	35 days (30 to 250 nm)
<b>Aqueous-phase chemistry</b>				
cloud-free			+ $10^{-9}$	> $10^4$ days
in cloud			+1.4	35 min (30 to 250 nm)

**Table 2** Results of the time scale analysis for the clean case (LAG1). Loss- and gain rates are given as maximum / minimum value over the observed period.

Process	Loss- / gain rates $dN / dt$ [ $1e-4 \text{ cm}^{-3} \text{ s}^{-1}$ ]	Total contribution in 26 hours [particles per $\text{cm}^3$ ]	Growth rates $dd / dt$ [ $\text{nm s}^{-1}$ ]	Growth time from $d_1$ to $d_2$
<b>Dry deposition</b>				
fine mode	-1.45 / -0.99	-11		
accumulation mode	-0.51 / -0.34	-4		
<b>Mixing</b>				
fine mode		-1145		
accumulation mode		-285		
<b>Sea-salt production</b>	+2.2 / +0.63	+11		
<b>Precipitation</b>				
fine mode	-224 / -213	-158		
accumulation mode	-16.8 / 16.5	-12		
		(2 hrs precipitation)		
<b>Diffusive coagulation of the fine mode</b>				
cloud-free	-5.95 / -5.82	-55		83 days (150 to 200 nm)
in cloud	-176 / 160	-241		5.7 days (150 to 200 nm)
		(4.0 hrs in cloud)		
<b>Self-coagulation</b>				
fine mode	-25 / 21	-215		227 days (60 to 200 nm)
accumulation mode	-0.90 / -0.88	-8		
<b>Condensation</b>			+0.5e-4	35 days (60 to 200 nm)
<b>Aqueous-phase chemistry</b>				
cloud-free			+7.03e-6	> $10^3$ days
in cloud			+2.64	2.3 min (60 to 200 nm)

**Table 3** Results of the time scale analysis for the polluted case (LAG2). Loss- and gain rates are maximum / minimum values over 26 hours.